JOURNAL OF COMPUTATIONAL PHYSICS 116, 173–179 (1995)

A Novel Hyperbolic Grid Generation Procedure with Inherent Adaptive Dissipation

C. H. TAI, S. L. YIN, AND C. Y. SOONG

Chung Cheng Institute of Technology, Taoyuan, Taiwan 33509, Republic of China

Received September 24, 1992; revised July 20, 1994

This paper reports a novel hyperbolic grid-generation with an inherent adaptive dissipation (HGAD), which is capable of improving the oscillation and overlapping of grid lines. In the present work upwinding differencing is applied to discretize the hyperbolic system and, thereby, to develop the adaptive dissipation coefficient. Complex configurations with the features of geometric discontinuity, exceptional concavity and convexity are used as the test cases for comparison of the present HGAD procedure with the conventional hyperbolic and elliptic ones. The results reveal that the HGAD method is superior in orthogonality and smoothness of the grid system. In addition, the computational efficiency of the flow solver may be improved by using the present HGAD procedure.

INTRODUCTION

In the past few decades numerical computation has become a powerful tool in the study of fluid dynamics and, especially, in the aerodynamics design of flying vehicles. Although the grid generation plays only a supporting role in computational fluid dynamics (CFD), it is also a crucial point in the efficiency and accuracy of the numerical predictions. Usually, grid clustering control is needed for high resolution of local areas, and orthogonality of the grid lines is particularly important for the calculations of the fluxes and gradients of the field properties. Generally speaking, there are two kinds of grid generation techniques, algebraic generation, and PDE (partial differential equations) generation of grids. The former is restricted to simple computational domains; the latter can be used for more complex configurations. According to the classification of the grid-generating PDE system, the PDE methods can be further divided into three categories, corresponding to elliptic systems of equilibrium type and parabolic and hyperbolic ones of marching (or propagation) type.

The elliptic grids can be generated by solving the Laplace or Poisson equation through an iterative procedure. The grid systems generated in this way have the merit of grid-density smoothness but with the penalty of time-consumption, while the orthogonality of the grid lines cannot be guaranteed. The hyperbolic grid generator includes orthogonality and cell-volume (or cell-area in two-dimensional cases) constraints and is solved by a marching procedure in a specified direction. This class of grid methods has the following features: (1) the surface grid distribution can be specified as desired; (2) the resulting grid system is orthogonal at the boundary and nearly so elsewhere; and (3) it is efficient in terms of computer time and memory for being non-iterative. The parabolic grid method lies between the elliptic and hyperbolic ones. A general discussion about various grid systems can be found in some review articles [1, 2].

Since the hyperbolic method is essentially a marching procedure, the specification of the entire boundary is not allowed and, therefore, the method is not appropriate for the computation of internal and closed flow systems. Nevertheless the hyperbolic method is very useful in the numerical investigations of external aerodynamics, for which the grid points are originally distributed only on the solid or inner boundary, and then are marched outward to construct the whole field grid until a sufficiently large far-field free boundary is reached. This class of methods works well, provided that the boundary is free from slope discontinuities. However, the geometric discontinuities at the inner boundaries may propagate into the grid field. Introducing artificial dissipation can reduce this drawback. Unfortunately, there is no general principle for the determination of the dissipation in numerical solution of such a hyperbolic system. Too small dissipation will not help prevent grid oscillations, but excess dissipation may cause crossing or overlapping of the grid lines.

Studies of hyperbolic grid generation can be traced back to the McNally–Graves procedure [3, 4]. Later on, Steger and Chaussee [5] presented the first systematic analysis of hyperbolic grid generation for two-dimensional configurations. The method was then extended to a three-dimensional (ξ, η, ζ) form with the use of dissipation terms in the ξ and η directions [6, 7]. A comparative study of algebraic, elliptic, and hyperbolic grids in PNS solutions of a hypersonic flow was performed by Kaul and Chaussee [8]. It was concluded that the shortest computational time was taken for flow solution on the hyperbolic grid system. By using a blunt body as an illustrative example, Hoffmann *et al.* [9] developed simple automatic procedures for grid control of two hyperbolic grid techniques, cell-

0021-9991/95 $6.00

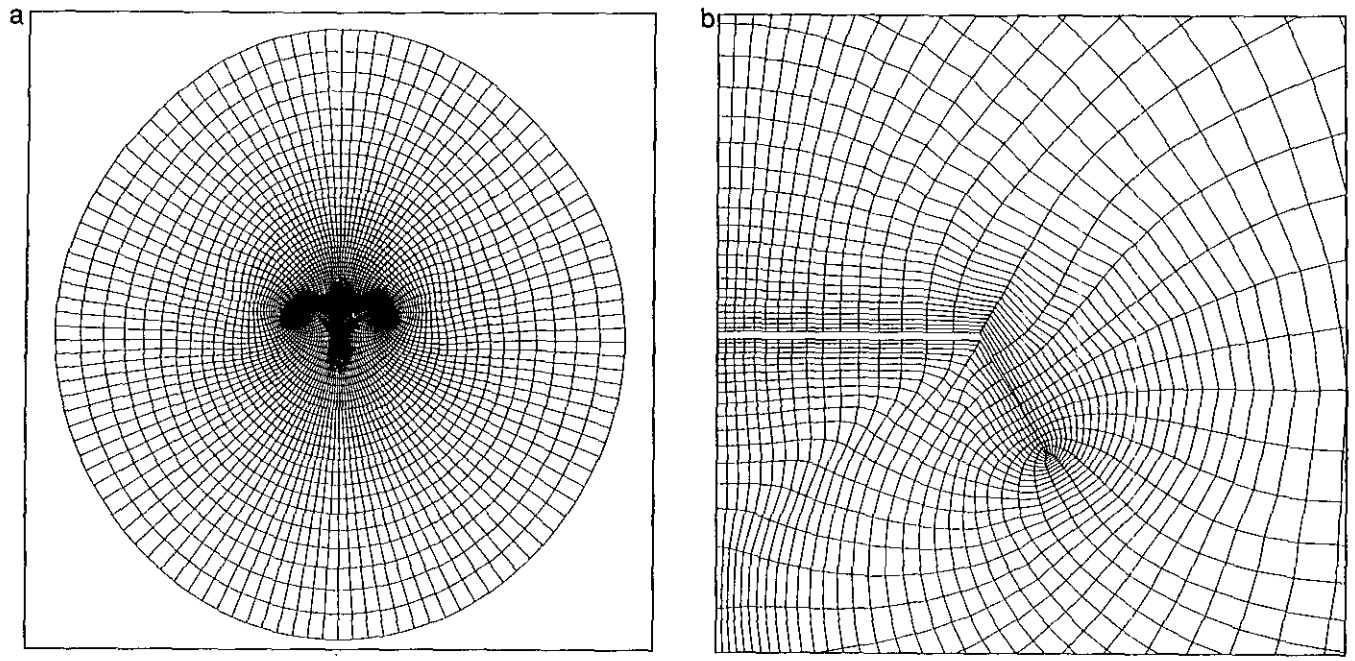

FIG. 1. HGAD grid around a cross section of delta-wing with 60° deflection of leading-edge vortex-flap (LEVF): (a) whole domain; (b) near-field grid.

area and arc-length schemes, proposed in Ref. [10]. Combination of hyperbolic grid generation with an adaptive strategy was studied by Klopfer [11].

In the present work the upwinding schemes [12], which have the merit of inherent dissipation, are applied to discretize the grid generator of hyperbolic nature. In the present study the inherent dissipation device is developed in the discretization. The dissipation is a field property and alters automatically. The tendency toward oscillation and overlapping of the grid lines can then be reduced. Configurations with geometric discontinuities and exceptional concavities are used as test cases for comparison of the present HGAD procedure and the conven-

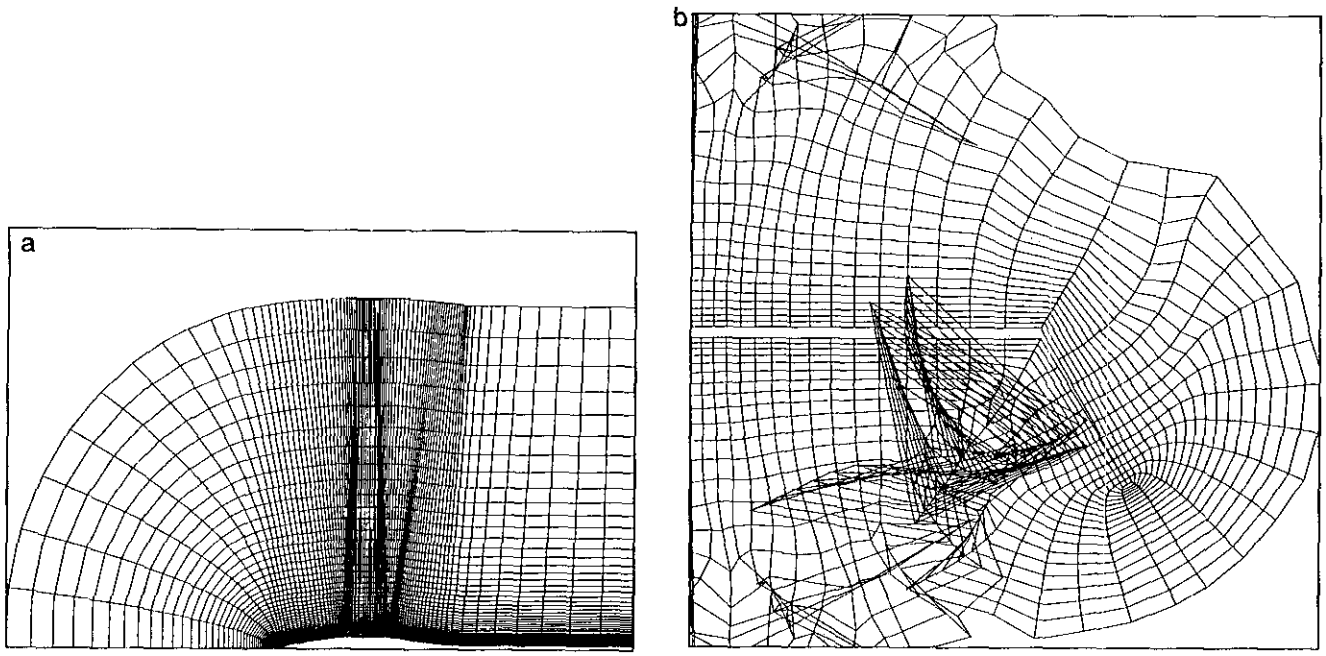

FIG. 2. Explicit hyperbolic grid for (a) axisymmetric projectile, (b) delta wing with 60° LEVF.

tional hyperbolic and elliptic ones. The computational efficiency is further examined by using the present HGAD procedure in the solution of a transonic flow field.

THEORETICAL ANALYSIS

The governing equations for two-dimensional grid generation are

$$x_\xi x_\eta + y_\xi y_\eta = 0 \tag{1}$$

$$x_\xi y_\eta - y_\xi x_\eta = V, \tag{2}$$

where x and y are the Cartesian coordinates in the physical plane, ξ and η are coordinates in the transformed plane, and V stands for the grid volume. Equations (1) and (2) are the orthogonality condition and the cell-volume control equations, respectively. After performing quasi-linearization on the system, one has

$$\mathbf{A}\mathbf{W}_\xi + \mathbf{B}\mathbf{W}_\eta = \mathbf{f}, \tag{3}$$

where

$$\mathbf{A} = \begin{bmatrix} x_\eta^0 & y_\eta^0 \\ y_\eta^0 & -x_\eta^0 \end{bmatrix}, \quad \mathbf{B} = \begin{bmatrix} x_\xi^0 y_\xi^0 \\ -y_\xi^0 x_\xi^0 \end{bmatrix}, \quad \mathbf{W} = \begin{bmatrix} x \\ y \end{bmatrix},$$

$$\mathbf{V} = \begin{bmatrix} 0 \\ V + V^0 \end{bmatrix}$$

in which x^0, y^0, and V^0 represent known values. Let the grid cells form and expand outward in the η-direction, Eq. (3) can then be cast into the form

$$\mathbf{W}_\eta + \mathbf{C}\mathbf{W}_\xi = \mathbf{S}. \tag{4a}$$

In Eq. (4a), $\mathbf{C} = \mathbf{B}^{-1}\mathbf{A}$, $\mathbf{S} = \mathbf{B}^{-1}\mathbf{V}$, and $\mathbf{C}$, α, and β are

$$\mathbf{C} = \frac{1}{x_\xi^{0^2} + y_\xi^{0^2}} \begin{bmatrix} \alpha & \beta \\ \beta & -\alpha \end{bmatrix}, \quad \alpha = x_\xi^0 x_\eta^0 - y_\xi^0 y_\eta^0,$$

$$\beta = x_\xi^0 y_\eta^0 + x_\eta^0 y_\xi^0.$$

The eigenvalues of matrix $\mathbf{C}$ are both real, i.e., $\lambda_{1,2} = \pm[(\alpha^2 + \beta^2)/(x_\xi^{0^2} + y_\xi^{0^2})]^{1/2}$ and $\lambda_1 = -\lambda_2 = \lambda$. This defines two diagonal matrices, viz. $\Lambda^+ = \mathrm{diag}[\lambda_1, 0]$ and $\Lambda^- = \mathrm{diag}[0, \lambda_2]$ such that $\Lambda = \Lambda^+ + \Lambda^-$ and $|\Lambda| = \Lambda^+ - \Lambda^-$. The Jacobian matrix $\mathbf{C}$ in Eq. (4a) can be expressed as $\mathbf{C} = \mathbf{C}^+ + \mathbf{C}^-$, where $\mathbf{C}^+ = \mathbf{R}\Lambda^+\mathbf{R}^{-1} = (\mathbf{C} + \lambda\mathbf{I})/2$ and $\mathbf{C}^- = \mathbf{R}\Lambda^-\mathbf{R}^{-1} = (\mathbf{C} - \lambda\mathbf{I})/2$. Accordingly, the relation $|\mathbf{C}| = \mathbf{C}^+ - \mathbf{C}^- = \lambda\mathbf{I}$ results.

Discretization by Upwind Scheme

Upon rewriting Eq. (4a) in conservation form

$$\mathbf{W}_\eta + \mathbf{F}_\xi = \mathbf{S}; \tag{4b}$$

and using the upwind schemes of Roe, Osher, and Steger-Warming [12], the corresponding flux ($\mathbf{F}$) formulas are

Roe,

$$\mathbf{F}(\mathbf{W}_\mathrm{R}, \mathbf{W}_\mathrm{L}) = \tfrac{1}{2}[\mathbf{F}(\mathbf{W}_\mathrm{L}) + \mathbf{F}(\mathbf{W}_\mathrm{R})] - \tfrac{1}{2}|\mathbf{C}|(\mathbf{W}_\mathrm{R} - \mathbf{W}_\mathrm{L}); \tag{5}$$

Osher,

$$\mathbf{F}(\mathbf{W}_\mathrm{R}, \mathbf{W}_\mathrm{L}) = \tfrac{1}{2}[\mathbf{F}(\mathbf{W}_\mathrm{L}) + \mathbf{F}(\mathbf{W}_\mathrm{R})] - \tfrac{1}{2}\int_{\mathbf{W}_\mathrm{L}}^{\mathbf{W}_\mathrm{R}} |\mathbf{C}|\, d\mathbf{W}; \tag{6}$$

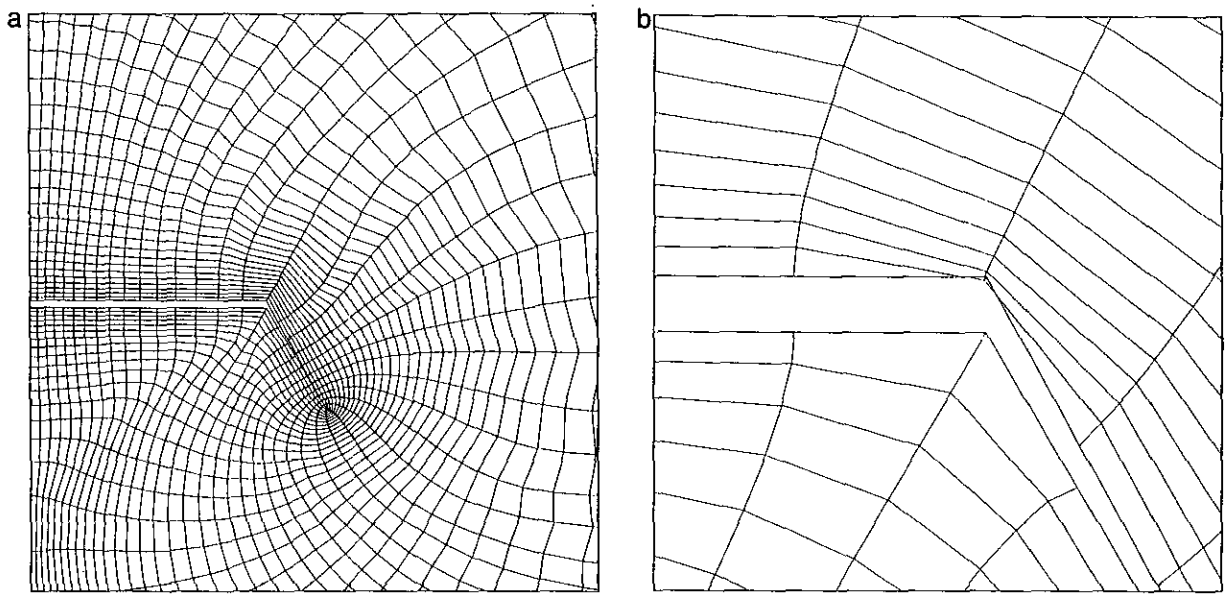

FIG. 3. Conventional hyperbolic grid with (a) $\varepsilon = 0$, (b) $\varepsilon = 0.3$.

Steger–Warming (flux-vector splitting, FVS),

$$\mathbf{F}(\mathbf{W}_R, \mathbf{W}_L) = \mathbf{C}^+\mathbf{W}_L + \mathbf{C}^-\mathbf{W}_R, \tag{7}$$

wherein $\mathbf{F}(\mathbf{W}_L) = \mathbf{C}\mathbf{W}_L$ and $\mathbf{F}(\mathbf{W}_R) = \mathbf{C}\mathbf{W}_R$. By setting $\Delta\xi = \Delta\eta = 1$ follows that $\mathbf{F}_\xi = \mathbf{F}_{i+1/2} - \mathbf{F}_{i-1/2}$. From Eqs. (5) and (6), Roe and Osher schemes, an identical form follows, viz.

$$\begin{aligned}\mathbf{F}_\xi = &\tfrac{1}{2}[(\mathbf{C}\mathbf{W}_{i+1} + \mathbf{C}\mathbf{W}_i) - |\mathbf{C}|_{i+1/2}(\mathbf{W}_{i+1} - \mathbf{W}_i)] \\ &- \tfrac{1}{2}[(\mathbf{C}\mathbf{W}_{i-1} + \mathbf{C}\mathbf{W}_i) - |\mathbf{C}|_{i-1/2}(\mathbf{W}_i - \mathbf{W}_{i-1})],\end{aligned} \tag{8}$$

while the FVS scheme gives

$$\mathbf{F}_\xi = (\mathbf{C}^+\mathbf{W}_i + \mathbf{C}^-\mathbf{W}_{i+1}) - (\mathbf{C}^+\mathbf{W}_{i-1} + \mathbf{C}^-\mathbf{W}_i) \tag{9}$$

which, by introducing the definitions of $\mathbf{C}^+$ and $\mathbf{C}^-$ into (9), again leads to Eq. (8). Substituting $\mathbf{F}_\xi$ and $(\mathbf{W}\eta)_i^n = \mathbf{W}_i^{n+1} - \mathbf{W}_i^n$ into (4b), an implicit form of discretization can be formulated,

$$\begin{aligned}-\tfrac{1}{2}\mathbf{C}\,\mathbf{W}_{i-1}^{n+1} + \mathbf{W}_i^{n+1} + \tfrac{1}{2}\mathbf{C}\,\mathbf{W}_{i+1}^{n+1} = \mathbf{S}_i^{n+1} + \mathbf{W}_i^n + \tfrac{1}{2}[|\mathbf{C}|_{i-1/2}\,\mathbf{W}_{i-1}^n \\ -(|\mathbf{C}|_{i-1/2} + |\mathbf{C}|_{i+1/2})\mathbf{W}_i^n + |\mathbf{C}|_{i+1/2}\mathbf{W}_{i+1}^n],\end{aligned} \tag{10}$$

in which $|\mathbf{C}|_{i+1/2} = \lambda_{i+1/2}$ and $|\mathbf{C}|_{i-1/2} = \lambda_{i-1/2}$ with the following options:

(a) $\lambda_{i-1/2} = \sqrt{\lambda_{i-1}\lambda_i}$, $\lambda_{i+1/2} = \sqrt{\lambda_i\lambda_{i+1}}$

(b) $\lambda_{i-1/2} = (\lambda_{i-1} + \lambda_i)/2$, $\lambda_{i+1/2} = (\lambda_i + \lambda_{i+1})/2$

(c) $\lambda_{i-1/2} = \lambda_{i+1/2} = \lambda_i$,

where (c) is a rather simple choice for evaluation of eigenvalue λ's. In the preliminary numerical tests, no significant difference was found in the computational results with the above three kinds of λ-evaluations. Therefore, by using (c), Eq. (10) can be written in a simple form,

$$\begin{aligned}-\tfrac{1}{2}\mathbf{C}\mathbf{W}_{i-1}^{n+1} + \mathbf{W}_i^{n+1} + \tfrac{1}{2}\mathbf{C}\mathbf{W}_{i+1}^{n+1} = \mathbf{S}_i^{n+1} + \mathbf{W}_i^n \\ + \frac{\lambda_i^n}{2}[\mathbf{W}_{i-1}^n - 2\mathbf{W}_i^n + \mathbf{W}_{i+1}^n].\end{aligned} \tag{11}$$

Adaptive Dissipation

The last term on right-hand side of Eq. (11) is an inherent second-order dissipation term. Examining the corresponding equations in the previous work, e.g., Ref. [5], the numerical dissipation term is artificially introduced and it may be second- or fourth-order, e.g.,

$$\begin{aligned}\text{artificial dissipation} &= \varepsilon(\Delta_i\nabla_i)\,\mathbf{W}_i^n \\ \text{or} \qquad &= \varepsilon(\Delta_i\nabla_i)^2\mathbf{W}_i^n\end{aligned} \tag{12}$$

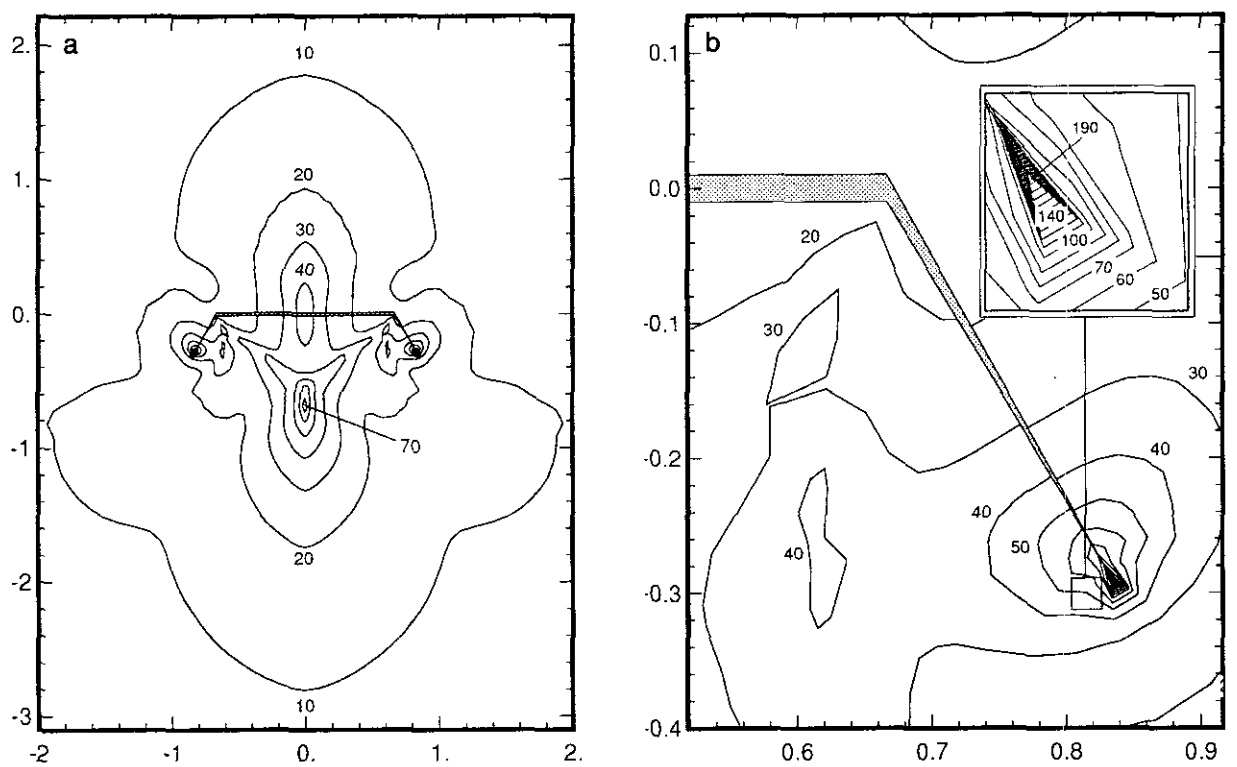

FIG. 4. Equi-dissipation contours for HGAD grid in Fig. 1: (a) near-field of the wing section; (b) close-up view near the wing-tip.

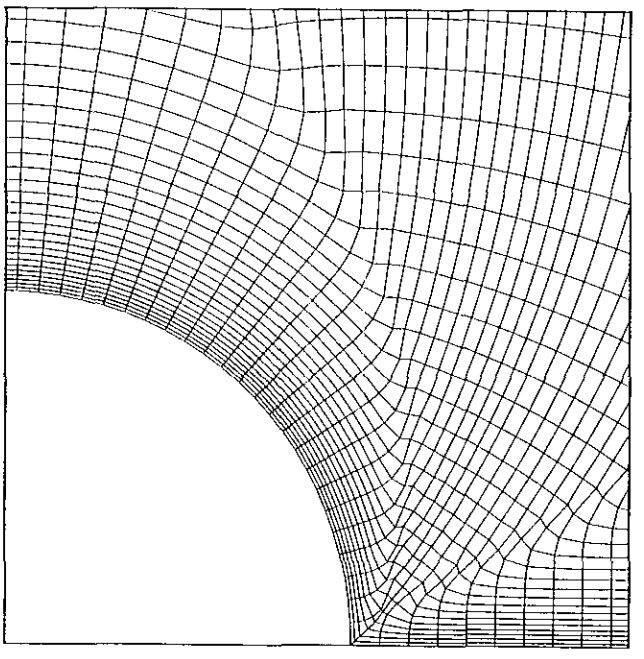

FIG. 5. HGAD grid with exceptional concavity.

wherein ε is the dissipation coefficient, chosen according to some slated rule, and Δ and ∇ are forward and backward difference operators, respectively. The present second-order dissipation term is called adaptive dissipation, i.e.,

$$\text{adaptive dissipation} = \tfrac{1}{2}\lambda_i^n(\Delta_i\nabla_i)\mathbf{W}_i^n, \tag{13}$$

and emerges from the analysis presented above. The adaptive dissipation coefficient λ_i^n is the eigenvalue of the Jacobian matric $\mathbf{C}$ which comes from the Euler-like equation (4b), and it can be calculated directly rather than arbitrarily chosen or guessed.

RESULTS AND DISCUSSION

Comparison of the Various Discretizations

In the discretization of the grid generation, the Jacobian matrix $\mathbf{C}$ is calculated by the use of the local information of the ith point rather than by using the signals coming from the neighboring points. In our experience, the calculation of $\mathbf{C}$ in the latter way may result overlap of the grid lines.

To study the effects of various discretizations, implicit and explicit, the two formulations

$$\begin{aligned} -\tfrac{1}{2}(\mathbf{C} + \lambda_i^n)\mathbf{W}_{i-1}^{n+1} + (\mathbf{I} + \lambda_i^n)\mathbf{W}_i^{n+1} + \tfrac{1}{2}(\mathbf{C} - \lambda_i^n)\mathbf{W}_{i+1}^{n+1} \\ = \mathbf{S}_i^{n+1} + \mathbf{W}_i^n \end{aligned} \tag{14}$$

and

$$\begin{aligned} \mathbf{W}_i^{n+1} = \tfrac{1}{2}(\mathbf{C} + \lambda_i^n)\mathbf{W}_{i-1}^n \\ + (\mathbf{I} - \lambda_i^n)\mathbf{W}_i^n - \tfrac{1}{2}(\mathbf{C} - \lambda_i^n)\mathbf{W}_{i+1}^n + \mathbf{S}_i^{n+1} \end{aligned} \tag{15}$$

are in addition to Eq. (11). Equation (14) is also implicit, with the dissipation terms at the $(n + 1)$th level and moved to the left-hand side, while Eq. (15) is essentially explicit.

Generally, the three formulations, Eqs. (11), (14), and (15),

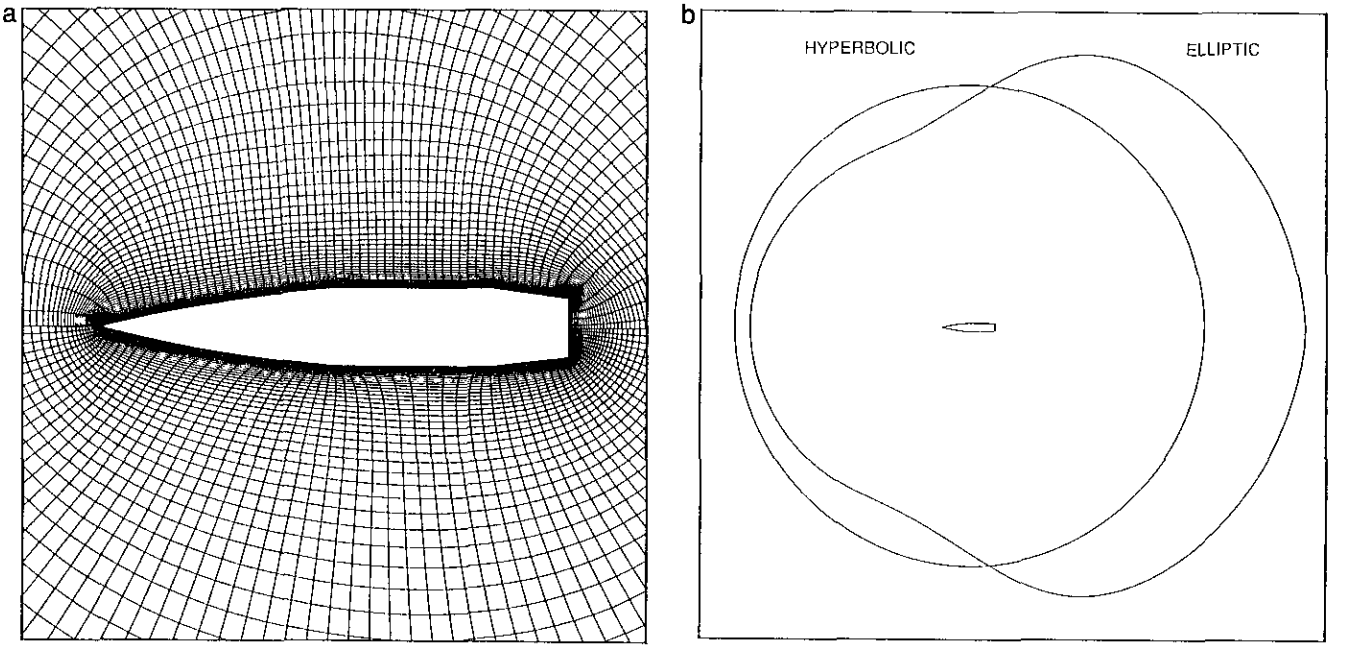

FIG. 6. Comparison of HGAD and elliptic grids: (a) near-fields of HGAD (upper half) and elliptic (lower half) grids; (b) outer boundaries.

all can produce acceptable grids for configurations of relatively smooth boundary. To examine the performance of the various discretizations, a cross section of a delta wing with 60° deflection of the leading-edge vortex flap is taken as an example. This two-dimensional configuration is a challenge to the grid generation for its features of concavity, convexity, sharp corner, and sharp edge. Equations (11) and (14) generate almost the same grid systems as shown in Fig. 1, and the resultant grid is fairly smooth, orthogonal and the clustering is also well controlled. Although the explicit scheme may work well as the implicit ones for a simple convex configuration such as ordnance projectile in Fig. 2a, it fails to generate an acceptable grid for the complex configuration shown in Fig. 2b. In summary, Eq. (11) is most desirable among the three and, therefore, the focus will be on this discretization in the remainder of the paper.

Comparison of the Inherent and Artificial Dissipations

Consider the artificial dissipation used in the conventional hyperbolic grid generation, Figs. 3a and 3b present the results for the same configuration with the dissipation factor $\varepsilon = 0$ and 0.3, respectively. Without dissipation, $\varepsilon = 0$, the grid lines oscillate especially in the far field as shown in Fig. 3a. For the case with $\varepsilon = 0.3$ in Fig. 3b, the oscillations are suppressed but the grid lines will deviate from the concave boundary and densely cluster to the convex corner. In the worst case, the grid lines may intersect with the convex boundary. The determination of the artificial dissipation is a crucial point for this class of hyperbolic grid generations; trial-and-error seems to be the only possible way to determine a proper value of the dissipation factor ε.

Alternatively, Fig. 4 presents the equi-dissipation (λ_i^η/V^0) contours for the hyperbolic grid shown in Fig. 1, which is generated by the present HGAD method. Since V^0 has been involved as a multiplier in the calculations of x_η^0 and y_η^0, the dissipation λ_i^η increases with the increasing V^0. To extract the real local dissipation, it is noted that λ_i^η is normalized by V^0. In Fig. 4a, it is observed that the inherent dissipation is a field property and varies point-by-point in the whole domain, and the values diminish as the grid grows toward far field. The larger values and gradients of the dissipation are presented in the near region beneath the wing. Figure 4b shows the close-up view of the dissipation contours near the tip region. For the extremely sharp edge, the relatively higher dissipation appears at the vicinity of the wing tip. Unlike the previous hyperbolic grid generations, however, the most striking feature of the present method is the adaptability of the dissipation device.

Specification of Cell Area

Specification of the cell area is an important factor for the growth of the whole grid system. Usually, a circle of the same peripheral length as the physical boundary is used for distributing points on the body. By setting the clustering function and the first-level cells adjacent to the boundary, the cell area can be controlled [5]. Just like the disturbance produced by a closed body on the water surface, the wave front near the body has a shape similar to that of the solid boundary, while the wave front approaches a circle as it propagates outward. The near-field wave front may become irregular if the solid body has geometric discontinuities and exceptional concavities, as the above-mentioned flapped wing. Although the dissipation is helpful, if the difference between the boundary slopes around the discontinuity is sufficiently large, the initial cell-area specification described above may fail to generate an acceptable grid. Under this circumstance, replacing the vertex or tip of the sharp corner or edge by two closely neighboring points is a valid way to alleviate the large slope-change on the boundary surface. Figure 1b is a successful example of this strategy. Alternatively, the first-level cell-area can be obtained by another method, e.g., the algebraic method, to obtain a better grid. In cases where cell-area control is extremely difficult, a special adjustment for some cells adjacent to the boundary may have to be employed. A few preliminary test runs are helpful for providing some clues to the determination of proper cell-area input. The use of this procedure is shown in the case of Fig. 5.

Numerical Computations on HGAD and Elliptic Grids

To evaluate the performance of the present HGAD grid, computations of the axisymmetric flow field around a secant-ogive-cylinder-bottail projectile at freestream Mach number 0.908 and Reynolds number 4.5×10^6 were carried out. The Navier–Stokes flow solver based on the Roe's upwinding devel-

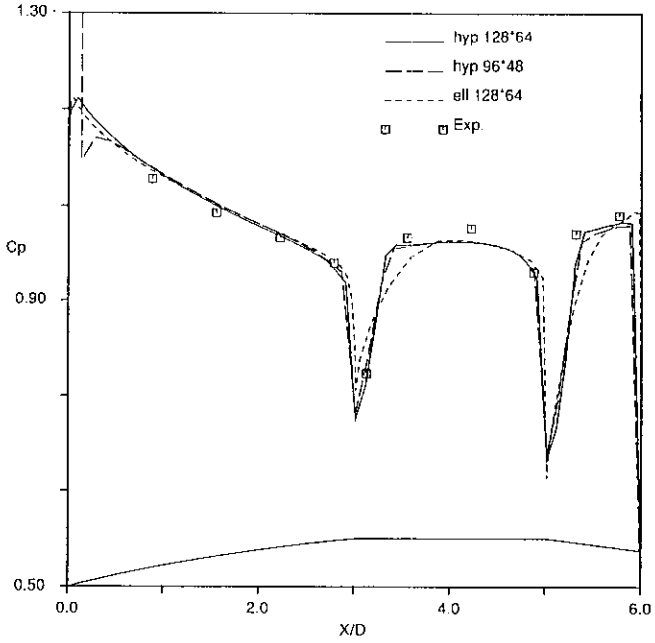

FIG. 7. Calculated and measured surface pressure distributions on the projectile at freestream Mach number = 0.908 and Reynolds number = 4.5×10^6.

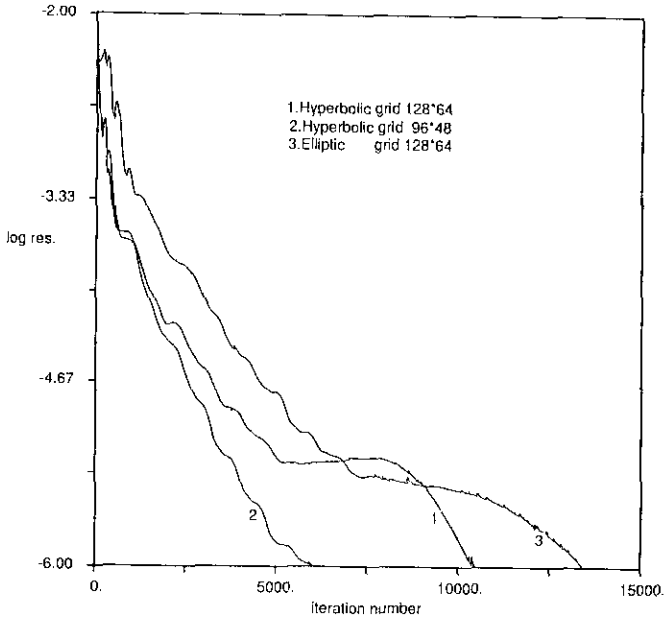

FIG. 8. Convergence history of flow solutions on various grids.

oped in a previous study [14] was used. The Baldwin–Lomax algebraic model was used for simulation of turbulence. The HGAD grids of 128 × 64 and 96 × 84 and the elliptic grid of 128 × 64 were employed for comparison. In Fig. 6a near-field hyperbolic and elliptic grids are presented in the upper and lower half planes, respectively. Obviously, the HGAD grid is of better orthogonality in the near-wall region. The outer boundaries for the two grid systems are shown in Fig. 6b. The calculated surface pressure distributions on the various grids are plotted in Fig. 7 and compared with the measured data [15]. Due to the sparseness of the grid near the projectile nose, the solution on the HGAD 96 × 84 grid presents a large discrepancy of surface pressure in the nose region. For the cases of the finer grids (128 × 64), the solution on HGAD is more accurate than that on the elliptic one. It is attributed to the characteristic of the orthogonality, which is of importance in the calculations of boundary vorticity and, in turn, in turbulence modeling.

Figure 8 shows the convergence history in the computations. It reveals that the computational efficiency can be improved by using the present HGAD grids.

CONCLUDING REMARKS

A novel hyperbolic grid generation procedure has been developed. Based on the above results the following conclusions can be drawn. Besides the non-iterative feature, the present HGAD method has the merits of inherent adaptive dissipation, resulting in better smoothness and orthogonality of the grid. These features improve the performance of the conventional hyperbolic grid schemes. A comparison between the numerical solutions on HGAD and elliptic grids demonstrates that the use of the HGAD grid in CFD cannot only improve accuracy but also computational efficiency. It is expected that the present HGAD method can also be extended to three-dimensional grid generation.

ACKNOWLEDGMENT

The authors gratefully acknowledge the financial support of the National Science Council of the Republic of China under the Grant NSC-82-0401-E-014-005.

REFERENCES

1. J. F. Thompson, *AIAA J.* **22,** 1505 (1984).
2. P. R. Eisenman, *Annu. Rev. Fluid Mech.* **17,** 487 (1985).
3. D. McNally, NASA TN D-6766, 1972 (unpublished).
4. A. Graves, Jr., NASA TM 80131, 1979 (unpublished).
5. J. L. Steger and D. S. Chaussee, *SIAM J. Sci. Stat. Comput.* **1,** 431 (1980).
6. J. L. Steger, AFSOR-TR-84-1022, 1984 (unpublished).
7. Y. M. Rizk, J. L. Steger, and D. S. Chaussee, NASA TM-86776, 1985 (unpublished).
8. U. K. Kaul and D. S. Chaussee, *Comput & Fluids* **13,** 421 (1985).
9. K. A. Hoffmann, W. H. Rutledge, and P. E. Rodi, in *Proceedings, Numerical Grid Generation in Computational Fluid Dynamics 1988*, edited by S. Sengupta *et al.* (Pineridge, Swansea, 1988), p. 147.
10. J. L. Steger and R. L. Sorenson, NASA CP-21666, 1980 (unpublished).
11. G. H. Klopfer, in *Proceedings, Numerical Grid Generation in Computational Fluid Dynamics 1988*, edited by S. Sengupta *et al.* (Pinebridge, Swansea, 1988), p. 443.
12. B. van Leer, J. L. Thomas, and P. L. Roe, AIAA-87-1104-CP, 1987 (unpublished).
13. C. J. Nietubicz, K. R. Heavey, and J. L. Steger, ARO Report 82-3, *Army Numerical Analysis and Computer Conference, 1982* (unpublished).
14. C. H. Tai and Y. L. Tian, *Chinese J. Mech.* **9**(3), 209 (1993).
15. L. D. Kayser and F. Whiton, ARBRL-MR-03161, 1982 (unpublished).